Fibroblast Inward-Rectifier Potassium Current Upregulation in Profibrillatory Atrial Remodeling

Xiao-Yan Qi,* Hai Huang,* Balazs Ordog, Xiaobin Luo, Patrice Naud, Yiguo Sun, Chia-Tung Wu, Kristin Dawson, Artavazd Tadevosyan, Yu Chen, Masahide Harada, Dobromir Dobrev, Stanley Nattel

Rationale: **Fibroblasts are involved in cardiac arrhythmogenesis and contribute to the atrial fibrillation substrate in congestive heart failure (CHF) by generating tissue fibrosis. Fibroblasts display robust ion currents, but their functional importance is poorly understood.**

Objective: **To characterize atrial fibroblast inward-rectifier K^+ current (I_{K1}) remodeling in CHF and its effects on fibroblast properties.**

Methods and Results: **Freshly isolated left atrial fibroblasts were obtained from controls and dogs with CHF (ventricular tachypacing). Patch clamp was used to record resting membrane potential (RMP) and I_{K1}. RMP was significantly increased by CHF (from −43.2±0.8 mV, control, to −55.5±0.9 mV). CHF upregulated I_{K1} (eg, at −90 mV from −1.1±0.2 to −2.7±0.5 pA/pF) and increased the expression of KCNJ2 mRNA (by 52%) and protein (by 80%). Ba^{2+} (300 μmol/L) decreased the RMP and suppressed the RMP difference between controls and dogs with CHF. Store-operated Ca^{2+} entry (Fura-2-acetoxymethyl ester) and fibroblast proliferation (flow cytometry) were enhanced by CHF. Lentivirus-mediated overexpression of KCNJ2 enhanced I_{K1} and hyperpolarized fibroblasts. Functional KCNJ2 suppression by lentivirus-mediated expression of a dominant negative KCNJ2 construct suppressed I_{K1} and depolarized RMP. Overexpression of KCNJ2 increased Ca^{2+} entry and fibroblast proliferation, whereas the dominant negative KCNJ2 construct had opposite effects. Fibroblast hyperpolarization to mimic CHF effects on RMP enhanced the Ca^{2+} entry. MicroRNA-26a, which targets KCNJ2, was downregulated in CHF fibroblasts. Knockdown of endogenous microRNA-26 to mimic CHF effects unregulated I_{K1}.**

Conclusions: **CHF upregulates fibroblast KCNJ2 expression and currents, thereby hyperpolarizing RMP, increasing Ca^{2+} entry, and enhancing atrial fibroblast proliferation. These effects are likely mediated by microRNA-26a downregulation. Remodeling-induced fibroblast KCNJ2 expression changes may play a role in atrial fibrillation promoting fibroblast remodeling and structural/arrhythmic consequences. (*Circ Res*. 2015;116:836-845. DOI: 10.1161/CIRCRESAHA.116.305326.)**

Key Word: arrhythmias, cardiac

Congestive heart failure (CHF) is an important cause of atrial fibrillation (AF), with structural remodeling, particularly tissue fibrosis, playing a central role.[1,2] Fibroblasts are the most abundant cells in the heart.[3] Fibroblast proliferation and differentiation into myofibroblasts are important contributors to arrhythmogenesis under conditions like CHF by enhancing the production of extracellular matrix proteins, such as collagen, and possibly via electric interactions with cardiomyocytes.[3]

Fibroblasts are known to express a wide range of ion channels, but their functional role is poorly understood.[3] Cardiac fibroblasts are not electrically excitable, but they have polarized resting membrane potentials (RMPs), with average values as negative as −37 mV.[4] The primary determinant of fibroblast RMP is the inward-rectifier K^+ current, I_{K1}.[5] We have recently shown that voltage-gated (Kv) K^+ currents in cardiac fibroblasts are remodeled in CHF.[6] This study aimed to characterize

Original received September 23, 2014; revision received January 16, 2015; accepted January 21, 2015. In December 2014, the average time from submission to first decision for all original research papers submitted to *Circulation Research* was 14.47 days.

From the Research Center and Department of Medicine, Montreal Heart Institute, Université de Montréal, Montreal, Quebec, Canada (X.-Y.Q., H.H., B.O., X.L., P.N., Y.S., C.-T.W., K.D., A.T., Y.C., M.H., S.N.); Department of Pharmacology and Therapeutics, McGill University, Montreal, Quebec, Canada (K.D., Y.C.); Department of Cardiology, Chang-Gung Memorial Hospital and University, Taoyuan, Taiwan, Republic of China (C.T.W., S.N.); Department of Cardiology, Fujita Health University School of Medicine, Toyoake, Japan (M.H.); and Institute of Pharmacology, Faculty of Medicine, University Duisburg-Essen, Essen, Germany (D.D.).

*These authors contributed equally to this article.

The online-only Data Supplement is available with this article at http://circres.ahajournals.org/lookup/suppl/doi:10.1161/CIRCRESAHA.116.305326/-/DC1.

Correspondence to Stanley Nattel, MD, Research Center, Université de Montréal, 5000 Belanger St E, Montreal, Quebec H1T 1C8, Canada. E-mail stanley.nattel@icm-mhi.org

Nonstandard Abbreviations and Acronyms

α-SMA	α-smooth muscle actin
AF	atrial fibrillation
AMO	anti-miR oligonucleotide
CHF	congestive heart failure
GFP	green fluorescent protein
KCNJ2-DN	dominant negative KCNJ2 construct
KCNJ2-OE	KCNJ2 overexpression
LA	left atrial
RMP	resting membrane potential

changes in cardiac fibroblast I_{K1} in CHF and to define underlying mechanisms and potential functional significance.

Methods

Animal Model

Adult mongrel dogs (22–30 kg) were divided into 2 groups: controls (28 males and 2 females) and dogs with 2-week ventricular tachypacing–induced congestive heart failure (CHF; 21 males and 3 females). Dogs with CHF had unipolar pacing leads inserted fluoroscopically into the right ventricular apex, which were programmed at 240 bpm for 2 weeks.[6] On study days, dogs were anesthetized with morphine (2 mg/kg subcutaneously) and α-chloralose (120 mg/kg intravenously, followed by 29.25 mg/kg per hour) and ventilated mechanically. Effective refractory periods were measured at basic cycle lengths of 150, 200, 250, 300, and 350 ms in the right-atrial appendage, with 10 basic stimuli (S1) followed by a premature extrastimulus (S2) with 5-ms decrements. AF was induced with atrial burst pacing at 50 Hz and 10 V. Mean AF duration was based on 10 AF inductions in each dog. If the mean duration of the first 5 episodes of AF was >2 minutes, AF was induced only 5 times. In 4 dogs per group, tissue sections were analyzed for fibrous-tissue content as previously described,[2] by an investigator blinded to group assignment.

Fibroblast Isolation and Culture

Atrial fibroblasts were obtained from left atria (LA) of adult mongrel dogs as previously described.[7] Hearts were removed after intra-atrial injection of heparin (10 000 U) and immersed in 2 mmol/L of Ca^{2+}-containing Tyrode solution. The left coronary artery was cannulated, and the LA tissue was perfused with 2 mmol/L of Ca^{2+} Tyrode solution (37°C, 100% O_2), then with Ca^{2+}-free Tyrode solution (≈10 minutes), followed by ≈60-minute perfusion with the same solution containing collagenase (≈0.48 mg/mL; CLSII, Worthington, OH) and 0.1% bovine serum albumin (Sigma). Cells were dispersed by trituration in KB (Kraftbruhe) solution (when used for electrophysiological study or sample acquisition for mRNA or protein analysis) or Medium 199 (Invitrogen) supplemented with 10% fetal bovine serum (Gibco), penicillin, and streptomycin for culture. Filtration (500-nm nanomesh) was used to remove debris, and cells were then centrifuged at 54.6*g* for 5 minutes to pellet cardiomyocytes. The supernatant was collected and filtered through 50-μm nanomesh and centrifuged at 314.5*g* for 10 minutes to concentrate fibroblasts. Freshly isolated fibroblasts were then separated; 1 aliquot was flash-frozen in liquid N_2 and stored for biochemical studies, and the remaining cells were cultured on noncoated glass coverslips.[7] Fibroblasts were incubated in 5% CO_2/95% O_2 humidified air (37°C). A medium change was performed 4 hours after plating to remove any dead cells and debris, and the medium was changed every 24 hours.

Ionic Current and RMP Recording

All in vitro recordings were obtained at 37°C. The whole-cell perforated–patch technique was used to record RMP in current-clamp mode, and tight-seal patch clamp was used to record I_{K1} in voltage-clamp mode. Borosilicate glass electrodes filled with pipette solution were connected to a patch-clamp amplifier (Axopatch 200A; Axon). Electrodes had tip resistances of 6 to 8 MΩ. Nystatin-free intracellular solution was placed in the tip of the pipette by capillary action (≈30 s), and then pipettes were backfilled with nystatin-containing (600 μg/mL) pipette solution. I_{K1} was recorded as the 300-μmol/L Ba^{2-}–sensitive current. Tyrode solution contained (mmol/L) NaCl 136, $CaCl_2$ 1.8, KCl 5.4, $MgCl_2$ 1, NaH_2PO_4 0.33, dextrose 10, and HEPES 5, titrated to pH 7.3 with NaOH. The pipette solution for RMP and I_{K1} recording contained (mmol/L) GTP 0.1, potassium aspartate 110, KCl 20, $MgCl_2$ 1, MgATP 5, HEPES 10, sodium phosphocreatine 5, and EGTA 0.005 (pH 7.4, KOH). Junction potentials between bath and pipette solutions averaged 10.5 mV and were corrected for RMP measurements only. Currents are expressed as densities (pA/pF) to control for changes in cell size/capacitance with CHF.

Ca^{2+} Imaging

One-day cultured canine atrial fibroblasts on microscope cover slips were loaded with Fura-2-acetoxymethyl ester (5 μmol/L; Invitrogen) in phenol-free M199 medium in the presence of Pluronic F-127 (20% solution in dimethylsulfoxide, 2.5 μg/mL) for 30 minutes at 36°C in a humidified incubator with 95% air/5% CO_2. Cover slips were fixed in a perfusion chamber on the stage of a microscope, and fibroblasts were superfused with 1.8 mmol/L of Ca^{2+} Tyrode solution and maintained for ≥25 to 30 minutes at room temperature before experimental protocols to allow for deesterification of Fura-2-acetoxymethyl ester. Fura-2 was excited with dual excitation wavelengths at 340 and 380 nm, and emission was recorded at a wavelength of 510 nm. Ca^{2+} imaging was obtained with an IonOptix Fluorescence System mounted on an upright Nikon FN-1 microscope. To measure store-operated Ca^{2+} entry, cells were first exposed to Ca^{2+}-free solution for 10 minutes. $[Ca^{2+}]_o$ was then increased to 10 mmol/L to measure Ca^{2+} entry via store-operated channels activated by Ca^{2+}-store depletion.

Cell Proliferation and Cell Cycle Analysis

Cell cycle was analyzed by flow cytometry as previously described.[8] Atrial fibroblasts were seeded at 4000 cells/cm^2 in T-25 culture flasks (1.0×10^5 cells per flask; 25 cm^2 growth area) and were cultured for 3 days in M199 medium supplemented with 10% fetal bovine serum. The culture medium was replaced with lentivirus-containing medium for each group on day 2. Cells were harvested after 48-hour incubation. After trypsinization, cells were centrifuged at 314.5*g* for 10 minutes and washed in ice-cold PBS, then fixed overnight in 75% ethanol and stored at −20°C until assayed. For analysis, stored samples were centrifuged at 314.5*g* for 10 minutes and washed twice in PBS. The pelleted samples were resuspended and incubated in propidium iodide (Sigma) solution for 20 minutes at 4°C. RNase was added in the staining solution to avoid RNA contamination. The stained fibroblast population was gated with forward scatter versus side scatter plot to display the relationship of cell size versus granularity. Data were acquired using a FACScan flow cytometer (BD Biosciences, San Jose, CA), with cell counts obtained during 5 minutes of flow at 60 μL/min, to create a DNA-content frequency histogram and analyzed with Flowjo software (Tree Star Inc). A Dean–Jett–Fox model was then used to quantify cell-cycle phases, giving the percentages of cells in G0/G1, S, and G2/M. The doublet problem was resolved by a doublet discrimination gate.

KCNJ2 Overexpression and Dominant Negative Constructs

Lentiviral constructs were used, carrying wild-type or dominant negative KCNJ2 cDNAs or pWPI-plasmid negative control expressing green fluorescent protein (GFP) only, as previously reported.[9] Lentivirus preparation was performed as previously described.[10] LA fibroblasts from control dogs were isolated and grown in T75 flasks. At near confluence (3–4 days of culture), fibroblasts were trypsinized, counted, and plated in 12-well plates at 4.4×10^4 cells per well. After 4 to 6 hours of recovery, cells were transduced with lentiviral vectors at 50 multiplicity of infection. After overnight incubation (≈15 hours), cells were washed 3× with 10% fetal bovine serum–containing medium. After an additional 48 hours of culture, electrophysiological studies, Ca^{2+} imaging, or flow cytometry was performed.

MicroRNA-26a Knockdown

For overexpression, sense and antisense oligonucleotides were synthesized by Invitrogen, and the double-stranded RNA was created by annealing. For knockdown, the anti-miR-26a oligonucleotide (AMO-26a) with locked nucleic acid chemistry was synthesized by Exiqon. Scrambled oligonucleotides with locked nucleic acid were used as negative controls (AMO-NC). LA fibroblasts of dogs in primary culture were transfected with AMO-26a (10 nmol/L) or AMO-NC (10 nmol/L) with Lipofectamine 2000 (Invitrogen). LA fibroblasts from control dogs were isolated and grown in T75 flasks. At near confluence (3–4 days of culture), fibroblasts were trypsinized, counted, and plated in 12-well plates at 4.4×10^4 cells per well. After 4 to 6 hours of recovery, cells were exposed to AMO-26a, AMO-NC, or vehicle in Lipofectamine. After overnight incubation, cells were washed 3× with 10% fetal bovine serum medium. After an additional 48 hours of transfection, cells were used for patch-clamp studies.

Taqman Real-Time Quantitative Reverse Transcription Polymerase Chain Reaction

Freshly isolated dog fibroblasts were resuspended in a lysis buffer, and RNA was isolated with Nucleospin RNA II (Macherey Nagel), including DNase treatment to prevent genomic contamination. Messenger RNAs were reverse-transcribed with the High-Capacity Reverse Transcription Kit (Applied Biosystems). Quantitative polymerase chain reaction was performed with TaqMan probes and primers from Applied Biosystems for housekeeping genes HPRT, β2-microglobulin, and G6PD, as well as for KCNJ2, collagen-1, collagen-3, fibronectin-1, fibrillin-1, and α-smooth muscle actin (α-SMA). SyBr green primers were used to quantify KCNJ12 and KCNJ4. The geometric mean expression of HPRT, β2-microglobulin, and G6PD was used for normalization. Quantitative polymerase chain reaction reactions were performed with Taqman Gene Expression Master Mix (Applied Biosystems). Reactions were run on a Stratagene MX3000. Relative gene expression values were calculated by the $2^{-\Delta Ct}$ method.

Immunostaining

Freshly isolated and cultured fibroblasts were rinsed with PBS and fixed for 10 minutes with 1:1 acetone:methanol at −20°C, and then cells were blocked for 1 hour with 5% bovine serum albumin at room temperature. The fibroblasts were incubated with mouse anti-α-SMA (1/500; Sigma), goat antivimentin (1/500; Santa Cruz), followed by donkey antimouse IgG-Alexa Fluor 555 (1/500; Invitrogen), donkey anti-rabbit IgG-Alexa Fluor 488 (1/500; Invitrogen), and TOPRO-3 iodide (1/1000; Invitrogen). Fluorescent images were obtained with an Olympus Fluoview FV1000 inverted confocal microscope.

Western Blots

Protein was extracted, quantified, and processed as we previously described.[8] Freshly isolated fibroblasts were lysed in detergent-based buffer (150 mmol/L NaCl, 20 mmol/L Tris–HCl, pH 7.4, 1 mmol/L EDTA, 1 mmol/L EGTA, 1% Nonidet P-40, 1% Triton X-100, 1 mmol/L NaF, 1 mmol/L Na_3VO_4, and protease inhibitors). Protein samples were separated by gel electrophoresis and transferred to polyvinylidene difluoride membranes. Membranes were blocked and incubated with mouse anti-α-SMA (1/1000; Sigma), goat antivimentin (1/1000; Santa Cruz), anti-Kir2.1 (1:200; Neuromab), and GAPDH (1/10 000; Fitzgerald) antibodies. Secondary antibodies conjugated to horseradish peroxidase were used for detection via chemiluminescence.

Data Analysis

Clampfit 9.2 (Axon), GraphPad Prism 4.0, and Origin 5.0 were used for data analysis. All data are expressed as mean±SEM. Multiple group statistical comparisons were obtained by 2-way ANOVA, and individual group mean differences were evaluated by Student *t* tests with Bonferroni correction. A 2-tailed $P<0.05$ was considered statistically significant.

Results

Properties of the Model

CHF significantly increased right-atrial effective refractory period at all basic cycle lengths (Online Figure IA). Mean AF duration increased substantially in dogs with CHF (Online Figure IB). CHF reduced arterial pressures and increased filling pressures (Online Figure IC–IE). Atrial histopathology confirmed the presence of fibrosis in dogs with CHF (Online Figure II), and quantitative polymerase chain reaction confirmed enhanced extracellular matrix gene expression (Online Figure IIIA and IIIB).

CHF-Induced Changes in Fibroblast Phenotype

Bright field microscopic images of freshly isolated fibroblasts from each group are shown in Figure 1A, with CHF fibroblasts being systematically larger (Figure 1B–1D). Immunoflorescence suggested that CHF fibroblasts exhibited enhanced vimentin and α-SMA expression (Figure 1E), an impression confirmed by image quantification (Figure 1F and 1G). Western blot analysis further supported CHF-induced fibroblast α-SMA and vimentin upregulation (Figure 1H and 1I). Gene expression mRNA levels corresponding to the extracellular matrix proteins collagen-1, collagen-3, fibronectin-1, and fibrillin-1 were all greater in freshly isolated CHF fibroblasts versus control fibroblasts (Online Figure IIIA and IIIB). These observations indicate that CHF alters atrial fibroblast phenotype.

Changes in I_{K1} and RMP

Figure 2A and 2B show examples of I_{K1} recordings from freshly isolated fibroblasts obtained with the ramp protocol shown in the inset. The current was strongly suppressed by 300 μmol/L Ba^{2+}. Overall data (Figure 2C) indicate significantly larger I_{K1} in CHF. CHF significantly increased the expression of KCNJ2 (Kir2.1) at both mRNA (by 52%) and protein (by 80%) levels (Figure 2D and 2E). KCNJ12 (Kir2.2) mRNA expression (Online Figure IIIC) was 2 orders of magnitude less than that of KCNJ2 (Online Figure IIID) and was not affected by CHF. KCNJ4 (Kir2.3) was undetectable. CHF significantly increased RMP (from −43.2±0.8 mV, control, to −55.5±0.9 mV; $P<0.001$; Figure 2F). Ba^{2+} (300 μmol/L) significantly reduced RMP and greatly attenuated the RMP differences between control and CHF fibroblasts, suggesting that they were due to I_{K1} upregulation in CHF (Figure 2F). Similar effects were seen with a 10-fold larger Ba^{2+} concentration (3 mmol/L; Figure 2G). Of note, despite the statistically significant reduction in RMP with Ba^{2+}, the fibroblasts maintained a negative RMP, indicating a contribution from conductances other than I_{K1}.

To further verify the role of I_{K1} in fibroblast RMP changes with CHF, we performed the studies shown in Online Figure IV. Consistent with expected behavior, the current conductance (and particularly the inward current component) was greatly enhanced (Online Figure IVA and IVB) by increasing extracellular K^+ concentration ($[K^+]_o$) to 75 mmol/L (equimolar substitution for Na^+). In addition to enhancing conductance (Online Figure IVC and IVD), increased $[K^+]_o$ shifted the reversal potential positively, from −53.4±3.7 mV and −64.3.7±3.8 mV with 5.4 mmol/L $[K^+]_o$ in controls and dogs with CHF, respectively, to −14.9±1.1 mV ($P<0.001$) and −15.1±1.1 mV

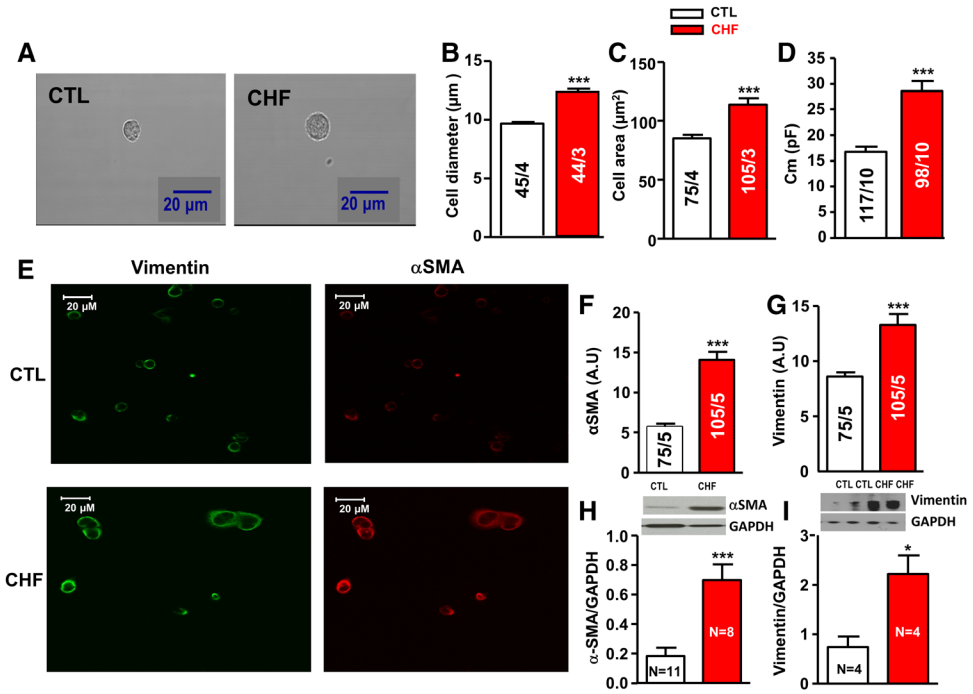

Figure 1. A, Microscopic images of freshly isolated fibroblasts from control (CTL) and congestive heart failure (CHF) canine left atria. **B–D**, Mean±SEM cell diameter, cell area, and cell membrane capacitance of CTL and CHF fibroblasts. **E**, Immunofluorescent images of freshly isolated CTL and CHF fibroblasts. Staining shown is vimentin (green) and α-SMA (red). **F–G**, Mean±SEM α-SMA and vimentin immunofluorescence quantification based on images like those in **E**. **H** and **I**, Mean±SEM α-smooth muscle actin (α-SMA) and vimentin immunoblot band intensities/GAPDH band intensities. *P<0.05 and ***P<0.001 CTL vs CHF; n/N=cells/dogs per group.

(P<0.001) in 75 mmol/L $[K^+]_o$. The RMP was significantly reduced by 75 mmol/L $[K^+]_o$ for both control and CHF conditions (Online Figure IVE and IVF) and elevating $[K^+]_o$ largely eliminated the RMP differences between controls and dogs with CHF, with values averaging −30.9±1.5 mV and −32.5±1.6 mV, respectively, in 75 mmol/L $[K^+]_o$ (P=not significant).

Changes in Fibroblast Ca^{2+} Entry

Figure 3A and 3B show store-dependent Ca^{2+} entry data from control and CHF fibroblasts, respectively. Cells in short-term (20 hours) culture were first exposed to nominally Ca^{2+}-free extracellular solution to deplete Ca^{2+} stores, and then Ca^{2+} entry was observed on increasing $[Ca^{2+}]_o$ to 10 mmol/L

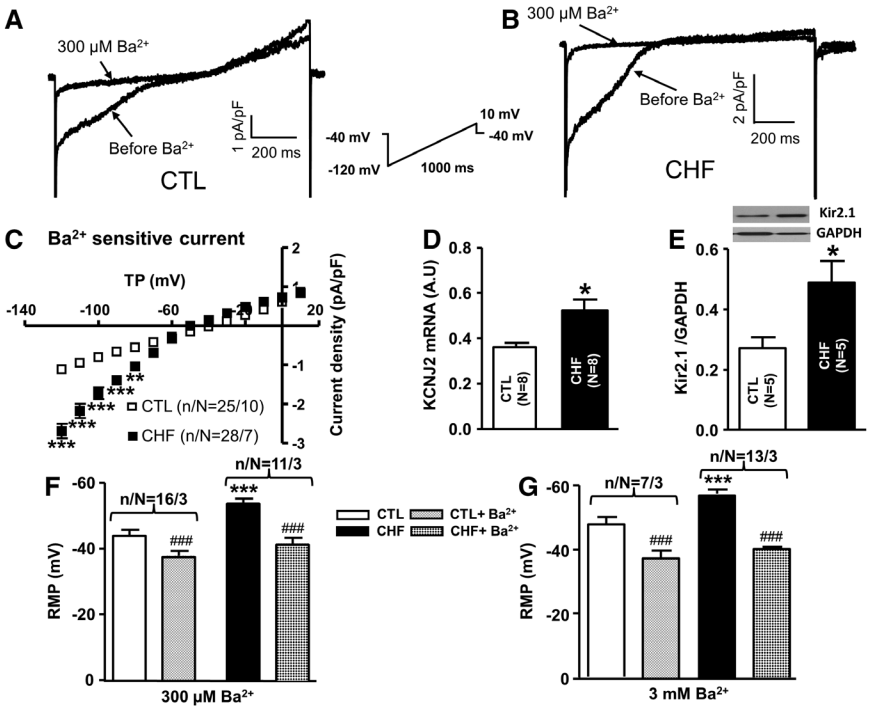

Figure 2. A and **B**, I_{K1} recordings (at 0.1 Hz) from control (CTL) and congestive heart failure (CHF) freshly isolated atrial fibroblasts. **C**, Mean±SEM current density vs voltage relationships for Ba^{2+} sensitive I_{K1} in freshly isolated atrial fibroblasts. **D**, Mean±SEM KCNJ2 mRNA expression. **E**, Mean±SEM Kir2.1 protein expression. **F** and **G**, Mean±SEM resting membrane potential (RMP) before and after 300 μmol/L or 3 mmol/L Ba^{2+}. *P<0.05, **P<0.01, and ***P<0.001 CTL vs CHF; ###P<0.001 pre-Ba^{2+} vs post-Ba^{2+}; n/N=cells/dogs per group. TP indicates test potential.

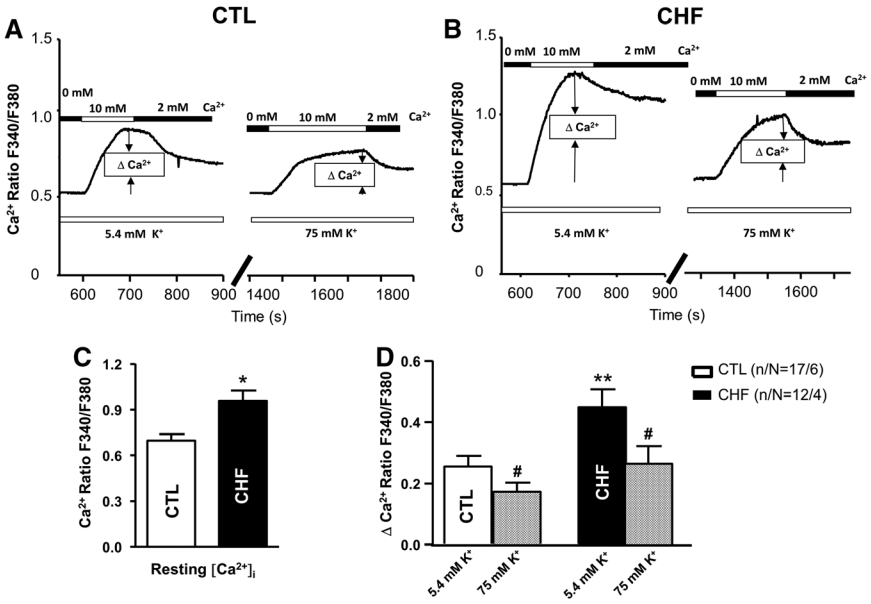

Figure 3. A and **B**, Recordings of store-operated Ca^{2+} influx in control (CTL) and congestive heart failure (CHF) freshly isolated atrial fibroblasts, in the presence of 5.4 mmol/L or 75 mmol/L $[K^+]_o$, with protocol shown at the top. **C**, Mean±SEM resting intracellular $[Ca^{2+}]$. **D**, Mean±SEM store-dependent Ca^{2+} influx. **P*<0.05, ***P*<0.01, CTL vs CHF; #*P*<0.05, 5.4 mmol/L $[K^+]_o$ vs 75 mmol/L $[K^+]_o$; n/N=cells/dogs per group.

(Figure 3A and 3B). Resting $[Ca^{2+}]_i$ (Figure 3C) and store-dependent Ca^{2+} entry (Figure 3D) were greater in CHF cells. We were unable to use Ba^{2+} as a probe to inhibit I_{K1} and study the role of I_{K1} differences in Ca^{2+} entry because Ba^{2+} interacts directly with Fura-2.[11] However, increasing $[K^+]_o$ to reduce RMP substantially suppressed store-dependent Ca^{2+} entry under both control and CHF conditions and greatly reduced the difference between control and CHF values (Figure 3D). These results suggest that RMP is a significant determinant of fibroblast Ca^{2+} entry and that RMP differences due to I_{K1} remodeling may contribute to the increased Ca^{2+} entry caused by CHF.

Fibroblast Proliferation and Differentiation

To study CHF-induced changes in fibroblast proliferation and differentiation, along with the potential contribution of I_{K1} remodeling, we had to perform experiments with short-term (3 days) cultured cells. We first verified that 3-day culture does not alter fibroblast I_{K1} or RMP (Online Figure V). We then collected fibroblasts for proliferation analysis by flow cytometry. Figure 4A and 4B show representative DNA-content histograms and Dean–Jett–Fox model fitting of control and CHF atrial fibroblasts (G0: resting phase; G1 phase: increased size and ready for DNA synthesis; G2/M phase: cells with doubled DNA content in premitotic and mitotic phases). CHF increased the total cell count and cell content in the G2/M phase (Figure 4C and 4D). Mean total cell counts are shown in Figure 4C and percentages in each phase in Figure 4D. CHF significantly increased the percentage of cells in the G2/M phase (Figure 4D), indicating increased proliferation. Cultured CHF fibroblasts also showed properties indicating greater myofibroblast differentiation versus control fibroblasts, including altered cell morphology and greater expression of vimentin and α-SMA protein (Online Figure VI).

I_{K1} Regulates RMP, Ca^{2+} Entry, and Proliferation

The experiments shown in Figure 3 suggest that I_{K1} may contribute to the control of atrial fibroblast Ca^{2+} entry. To explore the functional contributions of I_{K1} more directly, we used a gene transfer approach to vary the current in fibroblasts. A dominant negative KCNJ2 construct (KCNJ2-DN) with the GYG motif replaced by a triple-alanine (AAA) sequence

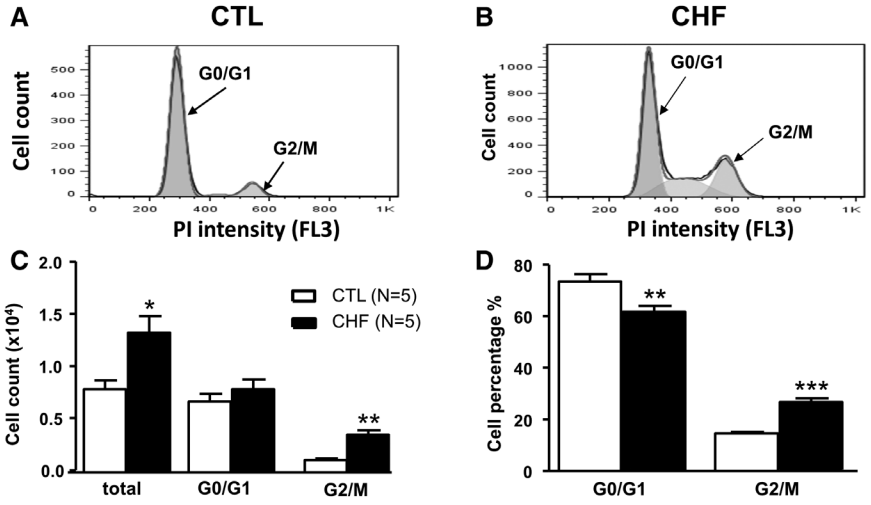

Figure 4. A and **B**, Representative DNA-content histograms and Dean–Jett–Fox model fitting of 3-day cultured atrial fibroblasts from a control (CTL) and a dog with congestive heart failure (CHF). **C**, Mean±SEM cell count of atrial fibroblasts from CTL and dogs with CHF. **D**, Mean±SEM percentage of cells in G0/G1 and G2/M phases. **P*<0.05, ***P*<0.01, and ****P*<0.001 CTL vs CHF. PI indicates propidium iodide.

was used to suppress endogenous KCNJ2 current. Wild-type KCNJ2 overexpression (KCNJ2-OE) was used to enhance the current. KCNJ2-DN and wild-type KCNJ2 were packed into a lentivirus vector containing GFP. A control virus was also prepared that contained only GFP inserted into the lentiviral vector. Infected cells were identified by green fluorescence.

Figure 5A shows original recordings of I_{K1} in fibroblasts infected with controls (lentivirus carrying GFP alone), KCNJ2-DN, and KCNJ2-OE constructs, before and after the addition of 300 μmol/L of Ba^{2+} to the superfusate. Currents were reduced by KCNJ2-DN and increased by KCN2-OE and strongly suppressed by Ba^{2+}. Figure 5B shows current–voltage relationships, with an inset showing control and KCNJ2-DN currents on an expanded current scale for clearer resolution. KCNJ2-OE greatly increased I_{K1}, whereas KCNJ2-DN strongly reduced I_{K1} density. Compatible with a role of I_{K1} in fibroblast differentiation, cell capacitance increased with KCNJ2-OE (Figure 5C). KCNJ2-OE substantially hyperpolarized the RMP, and consistent with the effects of Ba^{2+} shown in Figure 2F and 2G, KCNJ2-DN significantly reduced RMP. Exposure to Ba^{2+} eliminated the RMP differences among constructs (Figure 5D and 5E) with full effects seen at 300 μmol/L, consistent with the notion that the RMP differences are caused by changes in I_{K1}.

We then went on to use the gene transfer approach to confirm directly the ability of I_{K1} to regulate atrial fibroblast Ca^{2+} entry and proliferation. KCNJ2-DN decreased, and KCNJ2-OE increased, the resting Ca^{2+} level (Figure 6A) and store-operated Ca^{2+} entry (Figure 6B). Increased $[K^+]_o$ attenuated Ca^{2+} entry in the presence of the lentiviral-GFP control vector and KCNJ2-OE (Figure 6B), but as expected given the virtual elimination of I_{K1} produced by KCNJ2-DN, elevated $[K^+]_o$ did not alter Ca^{2+} entry in the presence of KCNJ2-KD. Fibroblast proliferation indices were enhanced by KCNJ2-OE and suppressed by KCNJ2-DN (Figures 6C and 6D). These results confirm the role of I_{K1} in governing fibroblast Ca^{2+} entry and proliferation.

Role of RMP in Controlling Fibroblast Ca^{2+} Entry

The most obvious way in which changes in I_{K1} could affect fibroblast Ca^{2+} entry is through resulting changes in RMP and the voltage gradient driving Ca^{2+} into the cell. To test directly the effect of RMP on fibroblast Ca^{2+} entry, we studied store-operated Ca^{2+} entry in fibroblasts under voltage-clamp conditions, with voltages set to approximate the RMP of control fibroblasts (−40 mV) and CHF fibroblasts (−55 mV). Figure 7A shows $[Ca^{2+}]_i$ recordings in one cell, obtained at a holding potential of −40 mV (left) and then in the same cell at −55 mV (right). Hyperpolarizing the fibroblast increased the Ca^{2+}-transient amplitude. Figure 7B shows the mean Ca^{2+}-transient amplitude in cells in which we were able to study Ca^{2+} entry under stable conditions under both voltages (order randomized in different cells). RMP had a highly significant effect on Ca^{2+}-transient amplitude.

MicroRNA-26 Regulation of Atrial Fibroblast I_{K1}

The larger increase in the KCNJ2 protein than mRNA in CHF points to mediation by microRNA. We have previously shown that miR-26 targets I_{K1} and that its downregulation in cardiomyocytes from animals with sustained AF governs cardiomyocyte I_{K1} enhancement.[12] We therefore considered the possibility that miR-26 regulation may contribute to the atrial fibroblast I_{K1} enhancement that we observed in CHF. Expression of the miR-26a isoform was decreased in freshly isolated LA fibroblasts from dogs with CHF, whereas miR-26b

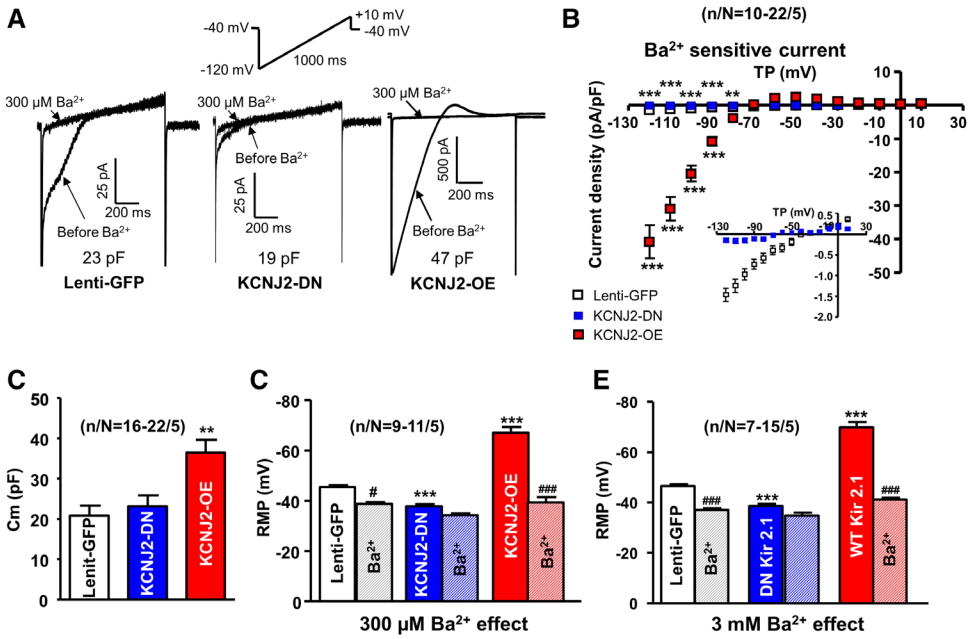

Figure 5. A, Representative I_{K1} recordings in green fluorescent protein (GFP)–expressing control (Lenti-GFP), KCNJ2 dominant negative (KCNJ2-DN), and KCNJ2–overexpressing (KCNJ2-OE) fibroblasts in primary culture. **B**, Mean±SEM Ba^{2+}-sensitive I_{K1} density–voltage relationships in cells infected with Lenti-GFP, KCNJ2-DN, and KCNJ2-OE vectors. Inset: Lenti-GFP and KCNJ2-DN data on enlarged current scale. **C**, Mean±SEM cell capacitance. **D** and **E**, Mean±SEM resting membrane potential (RMP) before and after 300 μmol/L and 3 mmol/L Ba^{2+}. $^{**}P<0.01$ and $^{***}P<0.001$ control vs Lenti-GFP. $^{\#}P<0.05$ and $^{\#\#\#}P<0.001$ pre-Ba^{2+} vs post-Ba^{2+}; n/N=cells/dogs per group. TP indicates test potential; and WT, wild-type.

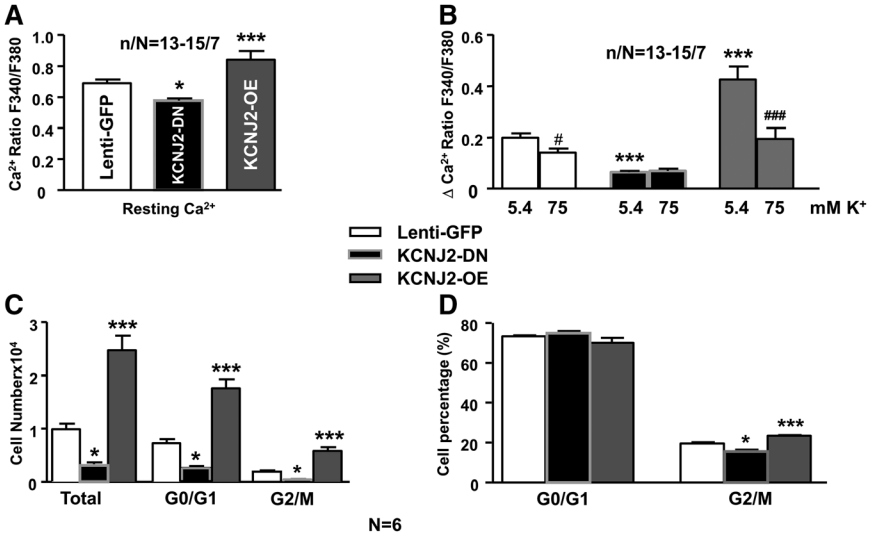

Figure 6. A, Mean±SEM resting intracellular [Ca^{2+}] in green fluorescent protein (GFP)–expressing control (Lenti-GFP), KCNJ2 dominant negative (KCNJ2-DN), and KCNJ2–overexpressing (KCNJ2-OE) fibroblasts. **B**, Mean±SEM Ca^{2+} influx (ΔCa^{2+}ratio) at 5.4 and 75 mmol/L $[K^+]_o$. **C**, Mean±SEM cell count of atrial fibroblasts in various phases from Lenti-GFP, KCNJ2-DN, and KCNJ2-OE groups. **D**, Mean±SEM percentage of cells in G0/G1 and G2/M phases. *P<0.05 and ***P<0.001 vs Lenti-GFP; #P<0.05 and ###P<0.001, 5.4 vs 75 mmol/L $[K^+]_o$; n/N=cells/dogs per group.

was unaffected (Figure 8A). AMO-26a transfection into atrial fibroblasts with lipofectamine effectively suppressed miR-26a (Figure 8B, left). To exclude nonspecific effects, we examined miR-21 expression, which was unaffected by AMO-26a (Figure 8B, right). We then looked at the result of knocking down miR-26a, to mimic its downregulation in CHF, on I_{K1} in atrial fibroblasts. Figure 8C shows original recordings from a fibroblast exposed to lipofectamine alone, a fibroblast exposed to a scrambled-control oligonucleotide (AMO-NC), and a fibroblast transfected with AMO-26a. I_{K1} was clearly larger after AMO-26a exposure, as indicated by the mean current–voltage data in Figure 8D. Finally, we examined the effect of miR-26a knockdown on atrial fibroblast RMP and noted substantial hyperpolarization (Figure 8E).

Discussion

In this study, we analyzed the consequences of CHF-induced I_{K1} upregulation in fibroblasts on fibroblast function, noting hyperpolarized RMP, enhanced Ca^{2+} entry, and increased proliferation indices. The mechanistic role of I_{K1} changes was supported by genetically modifying I_{K1} through KCNJ2-OE and knockdown, and the potential contribution of hyperpolarization to CHF-induced fibroblast Ca^{2+} entry increases was demonstrated by simultaneous voltage clamp and Ca^{2+} microfluorometry. CHF-induced miR-26a downregulation was implicated as the mechanism of KCNJ2/ I_{K1} upregulation.

Functional Role of Ion Channels in Cardiac Fibroblasts

Although the presence of ion channels in cardiac fibroblasts is well established,[3] their functional role is less clear. Ca^{2+} entry via nonselective cation channels of the transient receptor potential family plays a role in fibroblast proliferation, differentiation, and extracellular matrix protein secretion.[8,13] There is evidence that this action is mediated via Ca^{2+}-dependent activation of extracellular signal–related protein kinases[14] and contributes to the AF-related arrhythmogenic substrate.[8,13] The function of fibroblast K^+ channels is less clear. Previous work has indicated that Kir channels contribute to RMP determination. In cell coculture systems, myofibroblasts can be shown to couple to cardiomyocytes and alter their electrophysiological properties, inducing a variety of arrhythmogenic mechanisms.[14,15] Although the importance of fibroblast–cardiomyocyte coupling in vivo is still controversial, mathematical modeling work suggests that it may account for complex fractionated electrogram properties in fibrotic tissues.[16] We have recently evaluated the effects of fibroblast ion channel remodeling on the potential electric and arrhythmogenic interactions between coupled fibroblasts and cardiomyocytes, finding that if fibroblasts were well coupled to cardiomyocytes, fibroblast Kv current downregulation would suppress the AF-substrate, whereas Kir current upregulation would enhance

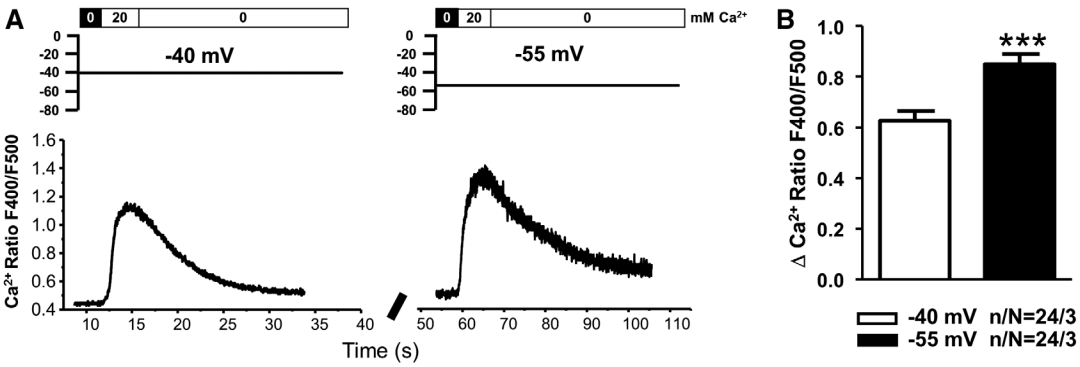

Figure 7. A, Original recordings of intracellular [Ca^{2+}] in one fibroblast held at –40 mV (left) and –55 mV (right) to mimic resting membrane potential in control and congestive heart failure fibroblasts. **B**, Mean±SEM Ca^{2+} influx (ΔCa^{2+}ratio) in 24 cells held at both –40 and –55 mV.

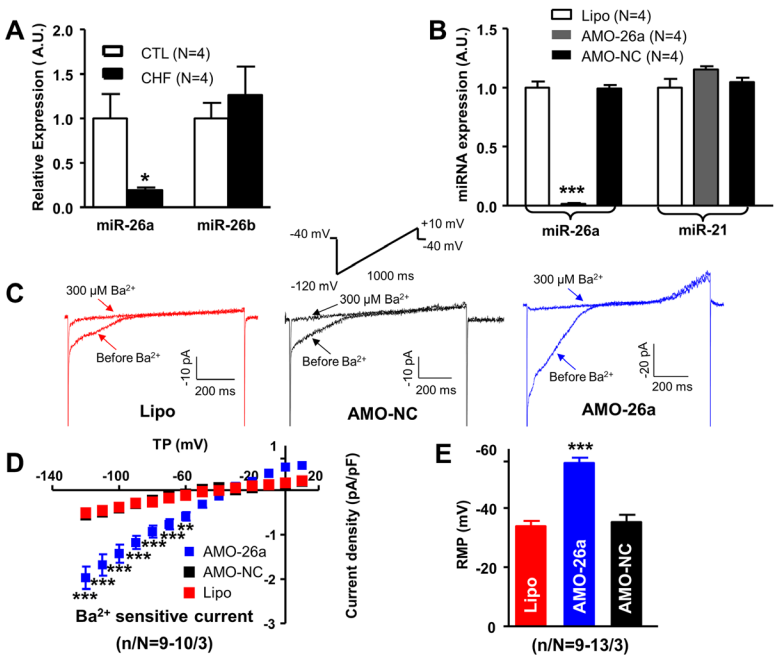

Figure 8. A, Mean±SEM relative microRNA expression in freshly isolated left atrial fibroblasts. **B**, Efficiency of miR-26a knockdown by anti-miR-26a oligonucleotide (AMO-26a) in canine left atrial fibroblasts. miR-21 was unaffected by AMO-26a. **C**, I_{K1} recordings (voltage-ramp protocol in the inset delivered at 0.1 Hz). **D**, Mean±SEM 300 μmol/L Ba^{2+}–sensitive I_{K1} density. **E**, Mean±SEM resting membrane potential (RMP). ***P*<0.01 and ****P*<0.001 Lipo vs AMO-26a; n/N=cells/dogs per group. AMO-NC indicates scrambled oligonucleotides with methylene bridges used as negative control for AMO-26a; CHF, congestive heart failure; CTL, control; and Lipo, lipofectamine control.

it.[17] We have also obtained evidence for a profibrotic role of Kv current downregulation, although the underlying mechanism is unclear.[6]

Control of Fibroblast Ca^{2+} Entry and Function by Kir Currents

This study is the first of which we are aware to show the control of fibroblast Ca^{2+} entry and proliferation by Kir2.1 current. Several lines of evidence converged to clarify the role of fibroblast I_{K1}. I_{K1} block with Ba^{2+} or K^+ driving force reduction by elevating $[K^+]_o$ reduced the RMP and elevated $[K^+]_o$ reduced fibroblast store-operated Ca^{2+} entry. Functional KCNJ2 knockdown with dominant negative overexpression reduced atrial fibroblast I_{K1}, RMP, Ca^{2+} influx, and proliferative activity, whereas KCNJ2-OE had the opposite effects. The role of RMP in mediating I_{K1} effects on Ca^{2+} entry was directly supported by experiments showing that hyperpolarization of voltage-clamped fibroblasts enhanced fibroblast store-operated Ca^{2+} entry.

Although this functional role has never before been described in fibroblasts, there is supportive evidence from previous work in endothelial cells. Bradykinin-induced changes in bovine endothelial cell cytosolic Ca^{2+} are consistent with an influx mechanism directly related to the Ca^{2+} electrochemical gradient.[18] Nitric oxide synthesis and proliferation of umbilical cord endothelial cells induced by basic fibroblast growth factor seem to depend on inward-rectifier K^+ current augmentation.[19] Finally, hyperpolarization increases cytoplasmic $[Ca^{2+}]$ in arteriolar endothelial cells.[20]

Novel Elements and Potential Significance

Cardiac fibrosis is an important contributor to cardiac dysfunction and arrhythmogenesis, and it is a particularly significant contributor to the substrate that allows enhanced AF maintenance in CHF.[21] Fibroblasts play a central role in the fibrotic process.[22] Here, we addressed a novel regulatory aspect of fibroblast physiology, functional control by I_{K1}, along with the remodeling of I_{K1} and its contribution to altered fibroblast function in a clinically relevant fibrotic paradigm: the CHF-induced atrial profibrillatory substrate.[1,2] We report for the first time that CHF-related atrial I_{K1} upregulation and consequent fibroblast hyperpolarization enhance fibroblast Ca^{2+} entry and cell proliferation. This work identifies a novel participant in the profibrotic response, with potential implications for the development of novel therapeutic interventions. Ion channels are targets for new antiarrhythmic agents.[23] Our study shows that in addition to altering cardiac electrophysiology, interventions that target I_{K1} may affect cardiac structural remodeling, particularly because the principal I_{K1} subunit, KCNJ2/Kir2.1, is common to both cardiomyocytes and fibroblasts. The predominance of KCNJ2 in cardiac I_{K1} is well recognized.[24] This study indicates that KCNJ2 is similarly predominant in fibroblasts: DN-KCNJ2 almost completely eliminated fibroblast I_{K1} (Figure 5B, inset). I_{K1} blockers are being developed as potential antiarrhythmic molecules,[25,26] based on their ability to inhibit cardiomyocyte I_{K1} and destabilize AF-maintaining rotors.[26,27] An additional potentially interesting consequence, based on the work reported here, might be the suppression of atrial fibrosis. The converse may also hold. Fibroblasts engineered to overexpress Kir2.1, Nav1.5, and connexin-43 subunits rescue normal propagation and decrease arrhythmia complexity in cocultured cardiomyocyte–fibroblast monolayers.[28] A risk of applying this approach therapeutically might be the profibrotic consequences of increased I_{K1}.

MicroRNAs are significant control molecules in cardiac remodeling.[29] We have previously shown that miR-26 downregulation contributes to AF-promoting remodeling by upregulating cardiomyocyte I_{K1}.[12] Here, we have identified an additional potential profibrillatory consequence of disease-related miR-26 downregulation: fibroblast activation via fibroblast I_{K1} upregulation consequent to removal of miR-26 induced negative regulation of the KCNJ2 gene.

Potential Limitations

Fibroblast hyperpolarization significantly increased store-operated Ca^{2+} entry by ≈30% (Figure 7B); however, CHF fibroblasts showed an ≈70% increase in Ca^{2+} entry (Figure 3D). Thus, the hyperpolarization caused by I_{K1} upregulation is likely not the only factor increasing Ca^{2+} entry in CHF fibroblasts. In addition to KCNJ2, miR-26 controls the expression of the gene encoding TRPC3 subunits.[8] TRPC3 subunit upregulation caused by miR-26 downregulation in AF enhances fibroblast Ca^{2+} entry.[8] Thus, TRPC3 expression changes caused by CHF-induced miR-26a downregulation likely also contributed to the increased fibroblast Ca^{2+} entry observed in CHF fibroblasts in this study.

We performed experiments in isolated fibroblasts to evaluate their cell biology in detail. Analysis of fibroblast properties in situ is greatly complicated by their small size and a dearth of specific probes. Paracrine effects in vivo could significantly alter fibroblast behavior and were not analyzed here. In addition, in this study we measured the fibrous-tissue content only in the LA appendage (Online Figure II). The distribution of fibrosis may not be uniform in atria.

Fibroblast proliferation might be affected by lentiviral infection. We therefore verified cell counts on culture in control fibroblasts versus lentivirus-GFP infected fibroblasts and found no significant differences (Online Figure VII).

We used Ba^{2+} as one of several tools to compare the contribution of I_{K1} in CHF fibroblasts with that in control. Ba^{2+} can affect a variety of K^+ currents, and the possibility of nonspecific effects requires caution in the interpretation of data. Evidence against any significant nonspecific effects of Ba^{2+} in our system is provided by the results of KCNJ2 knockdown on the response to Ba^{2+} (Online Figure VIII). Ba^{2+} had no significant effect on currents once KCNJ2/ I_{K1} was knocked down, indicating the absence of any significant effect on other currents under our recording conditions.

Acknowledgments

We thank Nathalie L'Heureux, Chantal St-Cyr, and Audrey Bernard for technical assistance and France Thériault for secretarial help with the article.

Sources of Funding

This work was supported by the Canadian Institutes of Health Research (44365, 6957) and the Heart and Stroke Foundation of Canada and the Fondation Leducq (European-North American Atrial Fibrillation Research Alliance; 07CVD03).

Disclosures

None.

References

1. Andrade J, Khairy P, Dobrev D, Nattel S. The clinical profile and pathophysiology of atrial fibrillation: relationships among clinical features, epidemiology, and mechanisms. *Circ Res*. 2014;114:1453–1468. doi: 10.1161/CIRCRESAHA.114.303211.
2. Li D, Fareh S, Leung TK, Nattel S. Promotion of atrial fibrillation by heart failure in dogs: atrial remodeling of a different sort. *Circulation*. 1999;100:87–95.
3. Yue L, Xie J, Nattel S. Molecular determinants of cardiac fibroblast electrical function and therapeutic implications for atrial fibrillation. *Cardiovasc Res*. 2011;89:744–753. doi: 10.1093/cvr/cvq329.
4. Kamkin A, Kiseleva I, Isenberg G. Activation and inactivation of a non-selective cation conductance by local mechanical deformation of acutely isolated cardiac fibroblasts. *Cardiovasc Res*. 2003;57:793–803.
5. Chilton L, Ohya S, Freed D, George E, Drobic V, Shibukawa Y, Maccannell KA, Imaizumi Y, Clark RB, Dixon IM, Giles WR. K^+ currents regulate the resting membrane potential, proliferation, and contractile responses in ventricular fibroblasts and myofibroblasts. *Am J Physiol Heart Circ Physiol*. 2005;288:H2931–H2939. doi: 10.1152/ajpheart.01220.2004.
6. Wu CT, Qi XY, Huang H, Naud P, Dawson K, Yeh YH, Harada M, Kuo CT, Nattel S. Disease and region-related cardiac fibroblast potassium current variations and potential functional significance. *Cardiovasc Res*. 2014;102:487–496. doi: 10.1093/cvr/cvu055.
7. Dawson K, Wu CT, Qi XY, Nattel S. Congestive heart failure effects on atrial fibroblast phenotype: differences between freshly-isolated and cultured cells. *PLoS One*. 2012;7:e52032. doi: 10.1371/journal.pone.0052032.
8. Harada M, Luo X, Qi XY, et al. Transient receptor potential canonical-3 channel-dependent fibroblast regulation in atrial fibrillation. *Circulation*. 2012;126:2051–2064. doi: 10.1161/CIRCULATIONAHA.112.121830.
9. Thomas J, Epshtein Y, Chopra A, Ordog B, Ghassemi M, Christman JW, Nattel S, Cook JL, Levitan I. Anthrax lethal factor activates K(+) channels to induce IL-1β secretion in macrophages. *J Immunol*. 2011;186:5236–5243. doi: 10.4049/jimmunol.1001078.
10. Dawson K, Wakili R, Ordog B, Clauss S, Chen Y, Iwasaki Y, Voigt N, Qi XY, Sinner MF, Dobrev D, Kaab S, Nattel S. MicroRNA29: a mechanistic contributor and potential biomarker in atrial fibrillation. *Circulation*. 2013;127:1466–1475. doi: 10.1161/CIRCULATIONAHA.112.001207.
11. Yamazaki J, Sato K, Ohara F, Nagao T. Direct activation of endothelial NO pathway by Ba^{2+} in canine coronary artery. *Br J Pharmacol*. 1998;124:1149–1158. doi: 10.1038/sj.bjp.0701948.
12. Luo X, Pan Z, Shan H, et al. MicroRNA-26 governs profibrillatory inward-rectifier potassium current changes in atrial fibrillation. *J Clin Invest*. 2013;123:1939–1951. doi: 10.1172/JCI62185.
13. Du J, Xie J, Zhang Z, Tsujikawa H, Fusco D, Silverman D, Liang B, Yue L. TRPM7-mediated Ca^{2+} signals confer fibrogenesis in human atrial fibrillation. *Circ Res*. 2010;106:992–1003. doi: 10.1161/CIRCRESAHA.109.206771.
14. Zlochiver S, Muñoz V, Vikstrom KL, Taffet SM, Berenfeld O, Jalife J. Electrotonic myofibroblast-to-myocyte coupling increases propensity to reentrant arrhythmias in two-dimensional cardiac monolayers. *Biophys J*. 2008;95:4469–4480. doi: 10.1529/biophysj.108.136473.
15. Rohr S. Arrhythmogenic implications of fibroblast–myocyte interactions. *Circ Arrhythm Electrophysiol*. 2012;5:442–452. doi: 10.1161/CIRCEP.110.957647.
16. Ashihara T, Haraguchi R, Nakazawa K, Namba T, Ikeda T, Nakazawa Y, Ozawa T, Ito M, Horie M, Trayanova NA. The role of fibroblasts in complex fractionated electrograms during persistent/permanent atrial fibrillation: implications for electrogram-based catheter ablation. *Circ Res*. 2012;110:275–284. doi: 10.1161/CIRCRESAHA.111.255026.
17. Aguilar M, Qi XY, Huang H, Comtois P, Nattel S. Fibroblast electrical remodeling in heart failure and potential effects on atrial fibrillation. *Biophys J*. 2014;107:2444–2455. doi: 10.1016/j.bpj.2014.10.014.
18. Laskey RE, Adams DJ, Johns A, Rubanyi GM, van Breemen C. Membrane potential and Na(+)–K^+ pump activity modulate resting and bradykinin-stimulated changes in cytosolic free calcium in cultured endothelial cells from bovine atria. *J Biol Chem*. 1990;265:2613–2619.
19. Scharbrodt W, Kuhlmann CR, Wu Y, Schaefer CA, Most AK, Backenköhler U, Neumann T, Tillmanns H, Waldecker B, Erdogan A, Wiecha J. Basic fibroblast growth factor-induced endothelial proliferation and NO synthesis involves inward rectifier K^+ current. *Arterioscler Thromb Vasc Biol*. 2004;24:1229–1233. doi: 10.1161/01.ATV.0000130663.37663.6a.
20. Dora KA, Garland CJ. Linking hyperpolarization to endothelial cell calcium events in arterioles. *Microcirculation*. 2013;20:248–256. doi: 10.1111/micc.12041.
21. Burstein B, Nattel S. Atrial fibrosis: mechanisms and clinical relevance in atrial fibrillation. *J Am Coll Cardiol*. 2008;51:802–809. doi: 10.1016/j.jacc.2007.09.064.
22. Souders CA, Bowers SL, Baudino TA. Cardiac fibroblast: the renaissance cell. *Circ Res*. 2009;105:1164–1176. doi: 10.1161/CIRCRESAHA.109.209809.
23. Nattel S, Carlsson L. Innovative approaches to anti-arrhythmic drug therapy. *Nat Rev Drug Discov*. 2006;5:1034–1049. doi: 10.1038/nrd2112.
24. Zaritsky JJ, Redell JB, Tempel BL, Schwarz TL. The consequences of disrupting cardiac inwardly rectifying K(+) current (I(K1)) as revealed by

the targeted deletion of the murine Kir2.1 and Kir2.2 genes. *J Physiol*. 2001;533:697–710.
25. Takanari H, Nalos L, Stary-Weinzinger A, de Git KC, Varkevisser R, Linder T, Houtman MJ, Peschar M, de Boer TP, Tidwell RR, Rook MB, Vos MA, van der Heyden MA. Efficient and specific cardiac I_{K1} inhibition by a new pentamidine analogue. *Cardiovasc Res*. 2013;99:203–214. doi: 10.1093/cvr/cvt103.
26. Filgueiras-Rama D, Martins RP, Mironov S, Yamazaki M, Calvo CJ, Ennis SR, Bandaru K, Noujaim SF, Kalifa J, Berenfeld O, Jalife J. Chloroquine terminates stretch-induced atrial fibrillation more effectively than flecainide in the sheep heart. *Circ Arrhythm Electrophysiol*. 2012;5:561–570. doi: 10.1161/CIRCEP.111.966820.
27. Pandit SV, Berenfeld O, Anumonwo JM, Zaritski RM, Kneller J, Nattel S, Jalife J. Ionic determinants of functional reentry in a 2-D model of human atrial cells during simulated chronic atrial fibrillation. *Biophys J*. 2005;88:3806–3821. doi: 10.1529/biophysj.105.060459.
28. Hou L, Hu B, Jalife J. Genetically engineered excitable cardiac myofibroblasts coupled to cardiomyocytes rescue normal propagation and reduce arrhythmia complexity in heterocellular monolayers. *PLoS One*. 2013;8:e55400. doi: 10.1371/journal.pone.0055400.
29. Kumarswamy R, Thum T. Non-coding RNAs in cardiac remodeling and heart failure. *Circ Res*. 2013;113:676–689. doi: 10.1161/CIRCRESAHA.113.300226.

Novelty and Significance

What Is Known?

- Cardiac fibroblasts play a central role in tissue fibrosis, which are an important contributor to a variety of arrhythmias, including atrial fibrillation.
- Cardiac fibroblasts possess a range of ion channels, but the functional role of fibroblast ion channels is poorly understood.
- Congestive heart failure (CHF) causes prominent atrial fibrosis, and is, therefore, a major risk factor for the arrhythmia.

What New Information Does This Article Contribute?

- CHF leads to the upregulation of the background inward-rectifier potassium current (I_{K1}) in atrial fibroblasts, likely by downregulating a microRNA (miR-26) that targets I_{K1}.
- An increase in atrial fibroblast I_{K1} hyperpolarizes the cell membrane, enhancing Ca^{2+} entry by increasing the driving force for transmembrane Ca^{2+} movement.
- These findings define a new pathway for CHF-induced atrial fibrosis involving an increase in I_{K1}, leading to hyperpolarization and enhanced Ca^{2+} entry and resulting in fibroblast activation.

CHF is an important clinical risk factor for atrial fibrillation, the commonest sustained arrhythmia and a major source of morbidity and mortality. Although CHF-induced atrial fibrosis is thought to contribute to the atrial fibrillation substrate, the mechanisms leading to this fibrosis are poorly understood. Moreover, the functional roles of ion channels in fibroblasts, the cells that produce fibrosis, are not well understood. Here, we studied changes in the background inward-rectifier potassium current (I_{K1}) in atrial fibroblasts from dogs with CHF induced by ventricular tachypacing. We found significant upregulation of I_{K1}, which hyperpolarized the resting membrane potential of the fibroblasts. This hyperpolarization enhanced Ca^{2+} entry, known to be an important fibroblast-activating mechanism, causing fibroblasts to proliferate. We also found that I_{K1} upregulation is caused by CHF-induced decreases in atrial fibroblast expression of a microRNA, miR-26, that targets the gene (*KCNJ2*) encoding I_{K1}. These findings reveal a new function of fibroblast potassium channels, ie, the control of fibroblast activation, and show that these channels can mediate a pathological arrhythmia–promoting response. Further elucidation of this signaling pathway would provide novel insights into the mechanisms controlling atrial fibrillation and might allow for the development of new therapeutic approaches.

Fibroblast Inward-Rectifier Potassium Current Upregulation in Profibrillatory Atrial Remodeling

Xiao-Yan Qi, Hai Huang, Balazs Ordog, Xiaobin Luo, Patrice Naud, Yiguo Sun, Chia-Tung Wu, Kristin Dawson, Artavazd Tadevosyan, Yu Chen, Masahide Harada, Dobromir Dobrev and Stanley Nattel

Circ Res. 2015;116:836-845; originally published online January 21, 2015;
doi: 10.1161/CIRCRESAHA.116.305326
Circulation Research is published by the American Heart Association, 7272 Greenville Avenue, Dallas, TX 75231

Print ISSN: 0009-7330. Online ISSN: 1524-4571

Supplemental Material

Fibroblast Inward-Rectifier Potassium Current Upregulation in Profibrillatory Atrial Remodeling

Xiao-Yan Qi, PhD,* Hai Huang, PhD,* Balazs Ordog, PhD, Xiaobin Luo, PhD, Patrice Naud, PhD, Yiguo Sun, PhD, Chia-Tung Wu, MD, Kristin Dawson, PhD, Artavazd Tadevosyan, PhD, Yu Chen, MSc, Masahide Harada, MD, PhD, Dobromir Dobrev, MD, Stanley Nattel, MD

* Both authors contributed equally

Supplemental Figures

Supplemental Figure 1

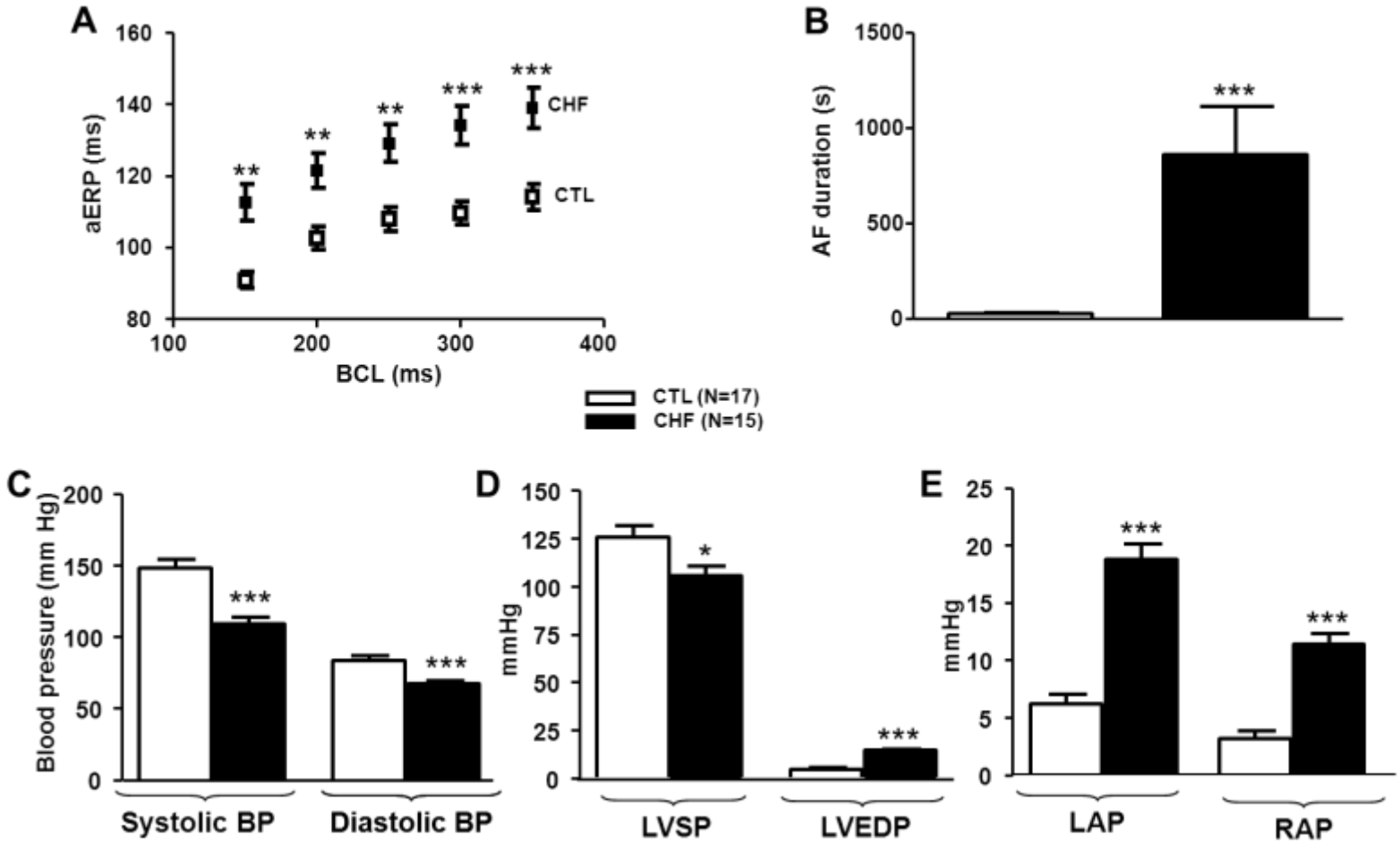

Supplemental Figure I. A, Mean±SEM atrial effective refractory period (ERP) as a function of basic cycle length (BCL). **B**, Mean±SEM duration of induced atrial fibrillation (AF) in control (CTL) and CHF. **C**, Mean±SEM blood pressure (BP). **D**, Mean±SEM left ventricular systolic pressure (LVSP) and left ventricular end diastolic pressure (LVEDP). **E**, Mean±SEM left atrial pressure (LAP) and right atrial pressure (RAP). **P*<0.05, ***P*<0.01, ****P*<0.001 vs CTL.

Supplemental Figure 2

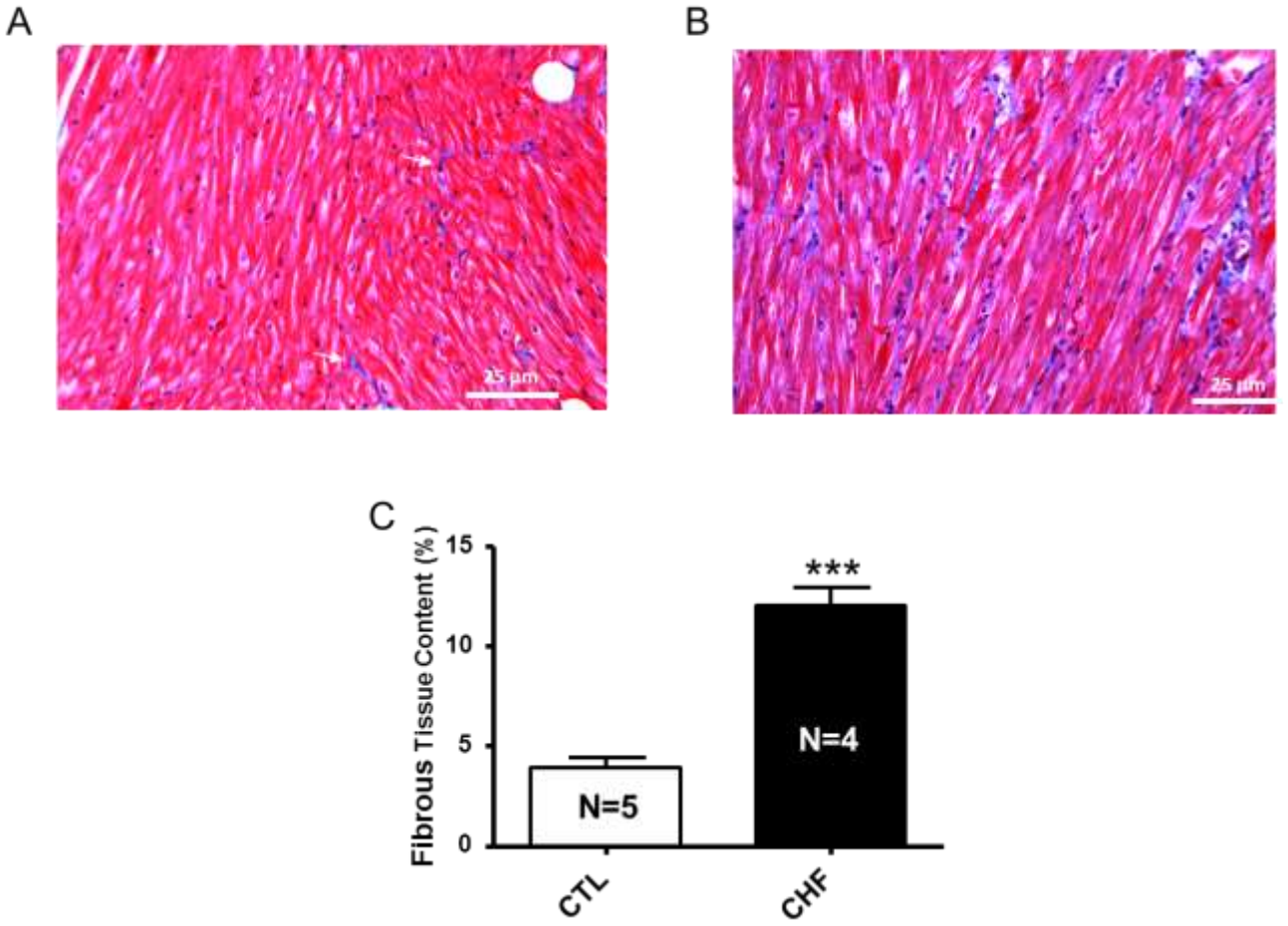

Supplemental Figure II. A-B, Masson's trichrome-stained light micrographs from a CTL (A) and a CHF (B) dog left atrial appendage (×200 magnification). **C**, Mean±SEM fibrosis tissue content (percentage of cross-sectional area) in left atrial appendage ***P<0.001 vs CTL.

Supplemental Figure 3

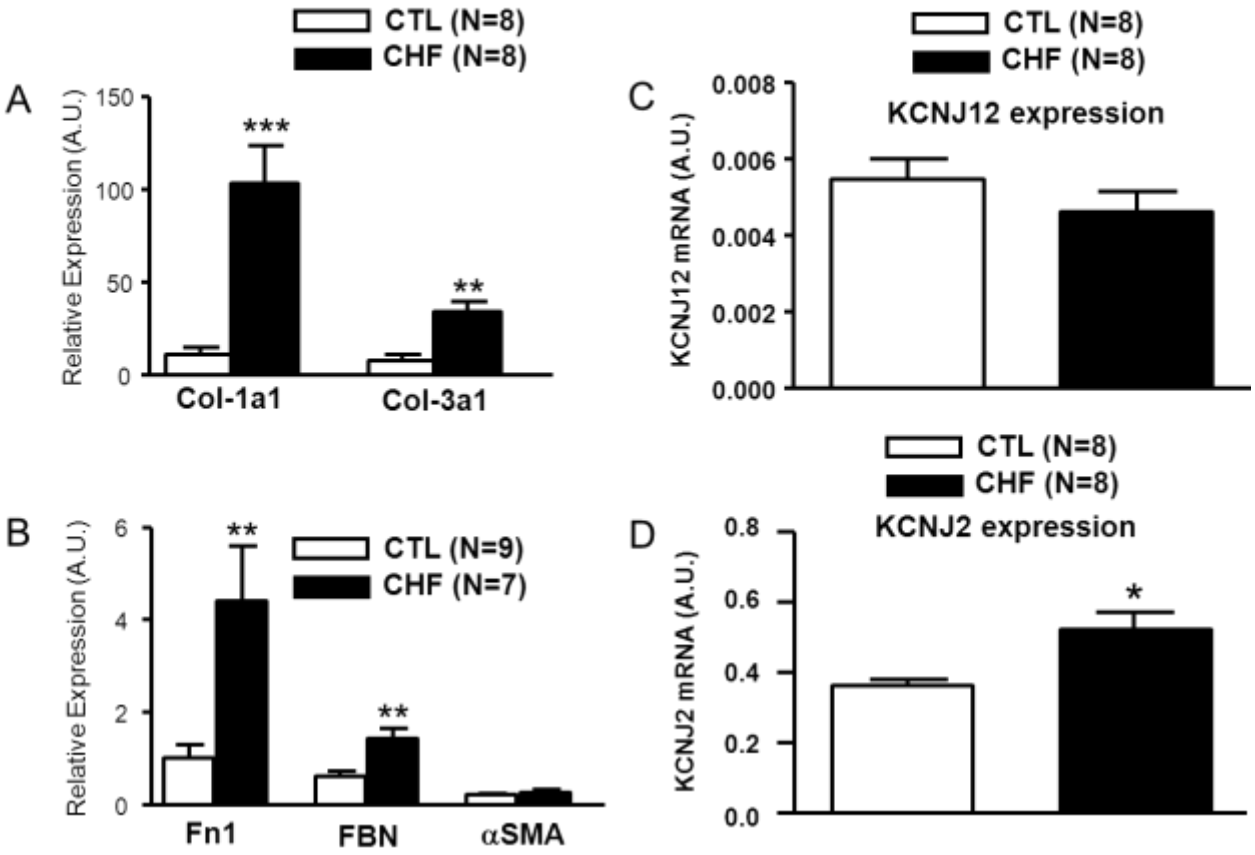

Supplemental Figure III. A-B, Mean±SEM extracellular matrix gene mRNA-expression in freshly-isolated atrial fibroblasts from CTL and CHF dogs. **C**, Mean±SEM KCNJ12 (Kir2.2) mRNA expression level. **D**, Mean±SEM KCNJ2 (Kir2.1) mRNA expression level. **P*<0.05, ***P*<0.01, ****P*<0.001 CTL vs CHF.

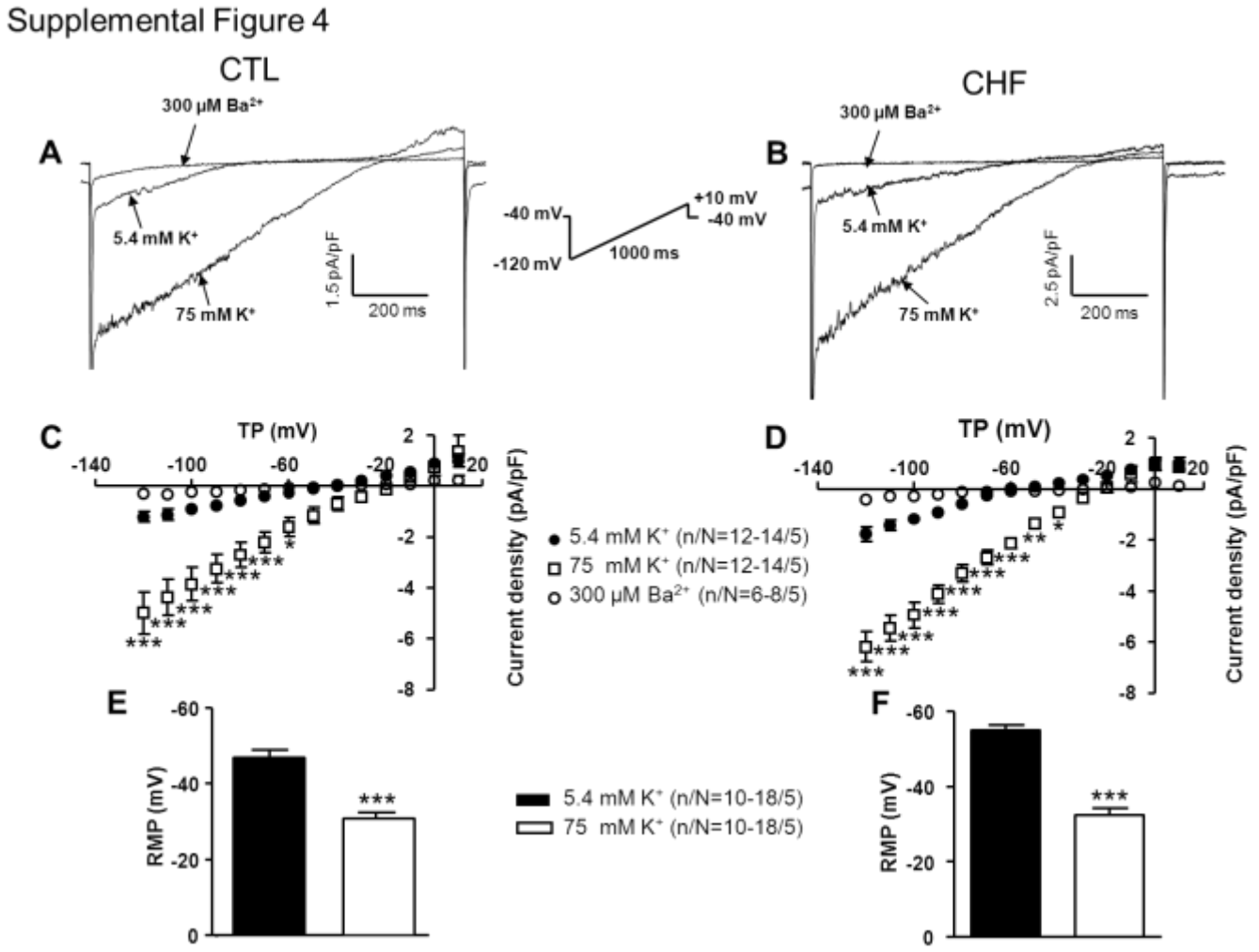

Supplemental Figure IV. A- B. Inwardly-rectifying K^+-current inward components are enhanced by 75 mol/L $[K^+]_o$ (reversal potential also shifted in the positive direction) and currents are blocked by 300 µmol/L Ba^{2+} in freshly-isolated CTL and CHF atrial fibroblasts. **C-D**, Mean±SEM inwardly rectifying K^+ current-density. **E-F**, Mean±SEM RMP in CTL and CHF freshly-isolated atrial fibroblasts before and after 75 mmol/L $[K^+]_o$-exposure. *,**, ***: P<0.05, 0.01, 0.001 for 5.4 mmol/L K^+ vs 75 mmol/L K^+, n/N=cells/dogs per group.

Supplemental Figure 5

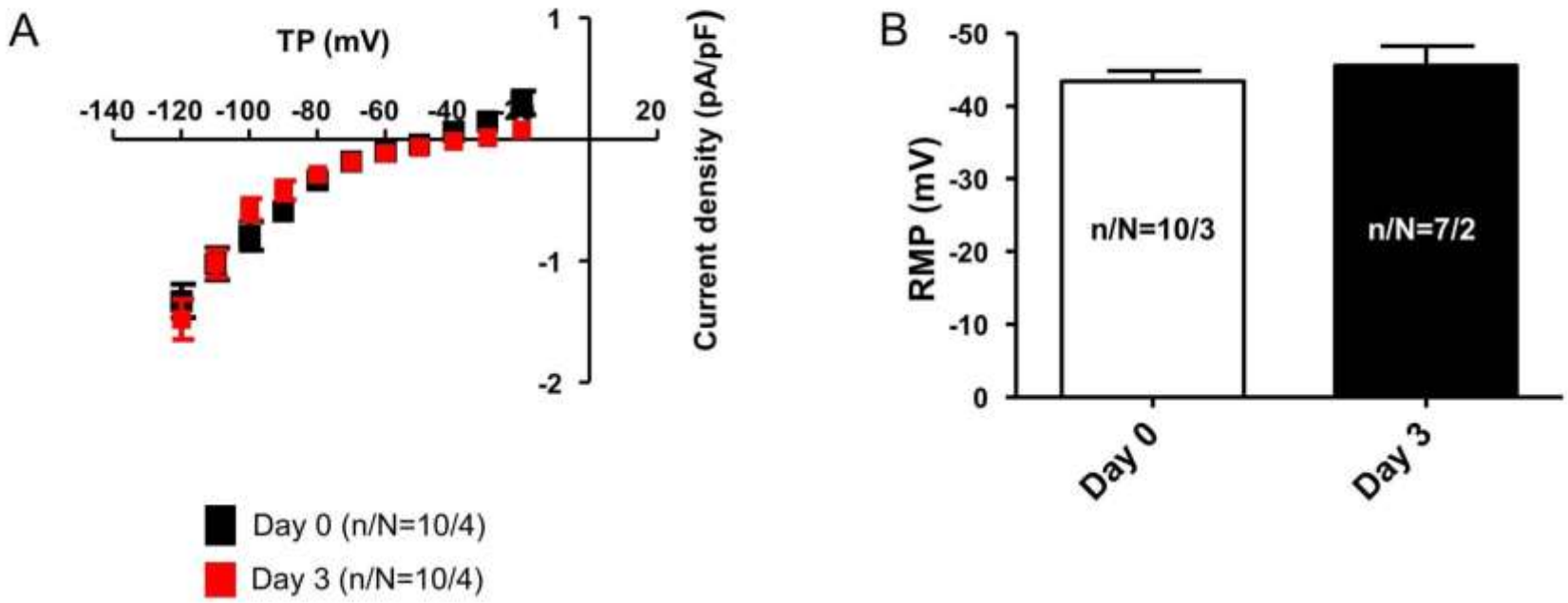

Supplemental Figure V. A, Mean±SEM current-voltage relations of Ba^{2+}-sensitive current from freshly-isolated and 3-day cultured atrial fibroblasts. **B**, Mean±SEM RMP from freshly-isolated and 3-day cultured atrial fibroblasts.

Supplemental Figure 6

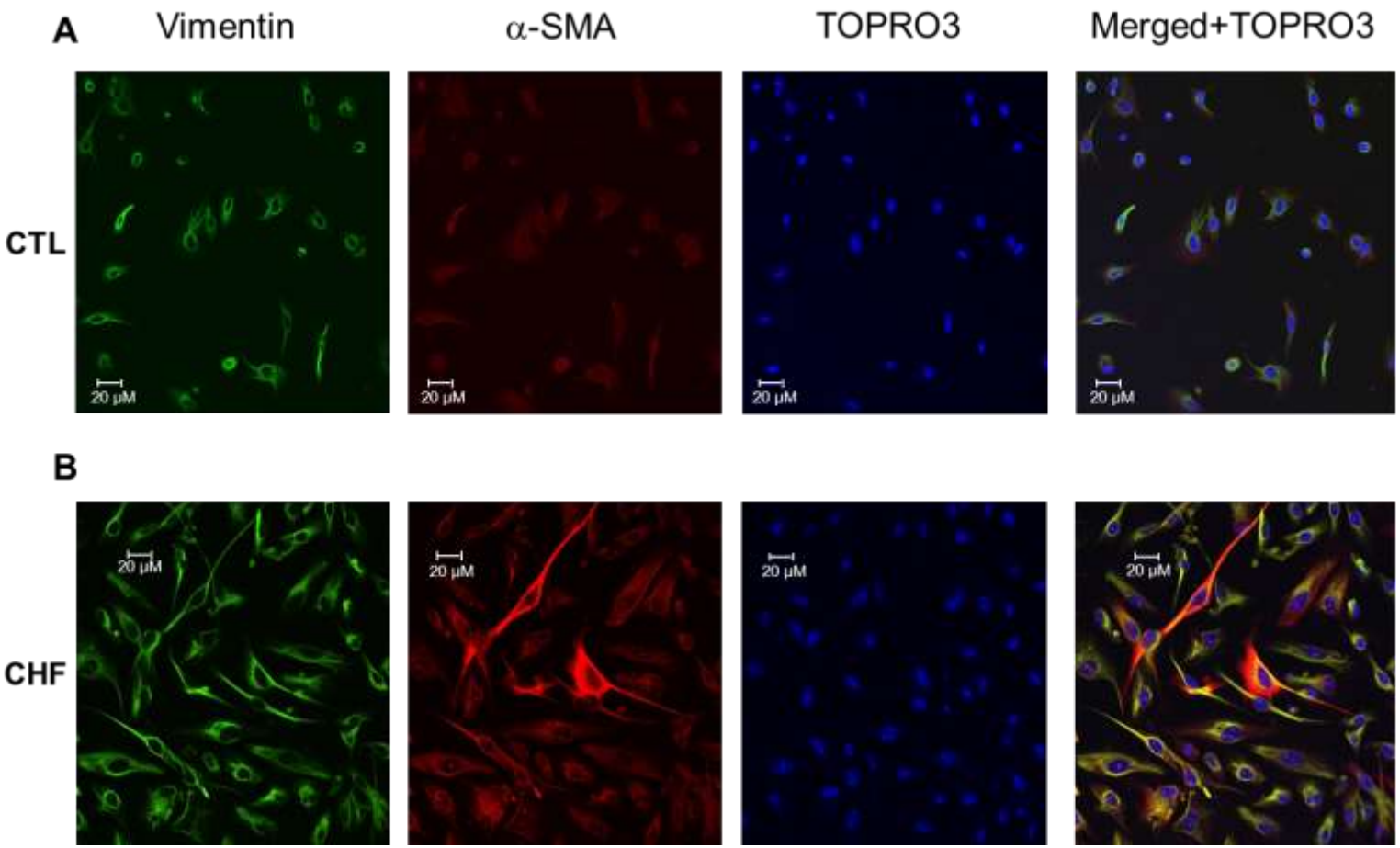

Supplemental Figure VI. A, Immunofluorescent images of 3-day cultured control (CTL) dog atrial fibroblasts. **B**, Immunofluorescent images of 3-day cultured CHF dog atrial fibroblasts. Staining shown is vimentin (green), α-SMA (red), TOPRO3 (blue, nuclear) and merged.

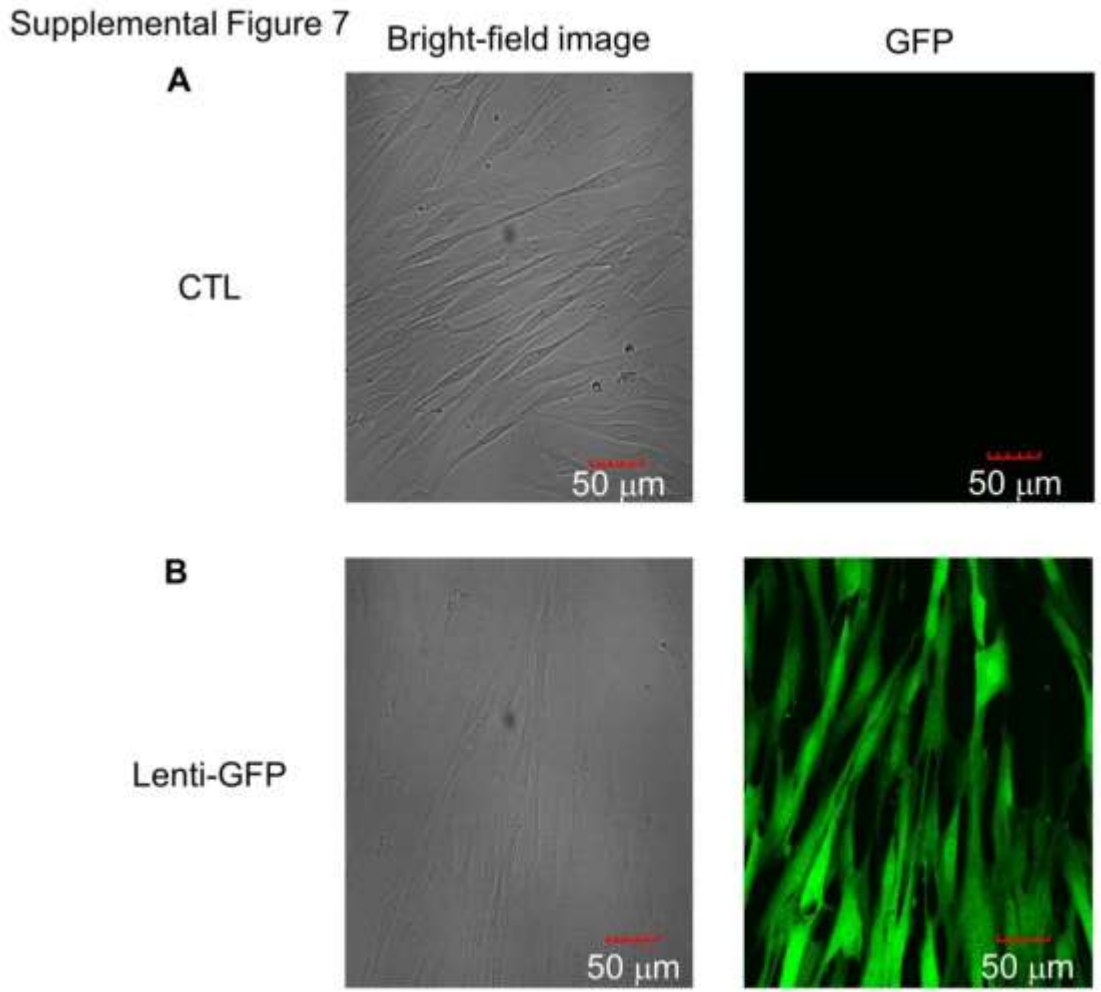

Supplemental Figure VII. Comparison of fibroblast proliferation in **A**, Control (CTL) fibroblasts and **B**, Lenti-GFP infected fibroblasts. Bright-field images are at left; fluorescent images are at the right. Cell counts after 3 days in culture were 58.2 ± 4.5/high-power field (HPF) for CTL versus 57.0 ± 3.2/HPF for Lenti-GFP (N=5, 6 respectively). To obtain cell counts, cells were cultured in the same general way as for flow cytometry, but rather than being passed through a flow cytometer, cells were counted visually under microscopy with a 40× objective lens.

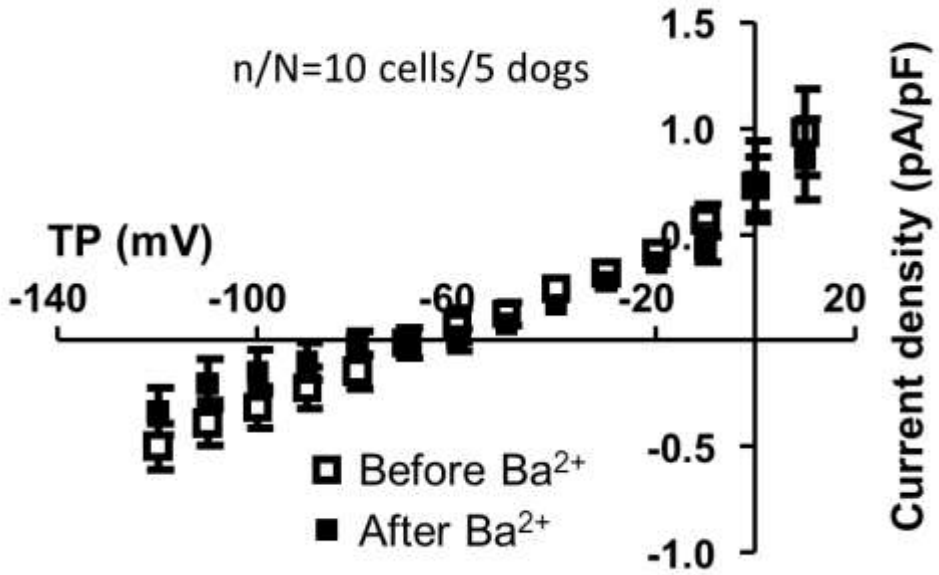

Supplemental Figure VIII. Currents measured in cells infected with KCNJ2-DN bearing lentivirus, before and after exposure to 300 µmol/L Ba^{2+}. Ba^{2+} had no statistically significant effect on these currents (2-way ANOVA, Ba^{2+} effect F=0.27, P=0.606).